Generation of narrow-bandwidth, tunable, coherent xuv radiation using high-order harmonic generation

Jinping Yao,[1,2] Ya Cheng,[1,*] J. Chen,[3,4,†] Haisu Zhang,[1,2] Han Xu,[1] Hui Xiong,[1] Bin Zeng,[1,2] Wei Chu,[1,2] Jielei Ni,[1,2] X. Liu,[5] and Zhizhan Xu[1,‡]

[1]*State Key Laboratory of High Field Laser Physics, Shanghai Institute of Optics and Fine Mechanics, Chinese Academy of Sciences, P.O. Box 800-211, Shanghai 201800, China*

[2]*Graduate University of Chinese Academy of Sciences, Beijing 100049, China*

[3]*Center for Applied Physics and Technology, Peking University, Beijing 100084, China*

[4]*Institute of Applied Physics and Computational Mathematics, Beijing 100088, China*

[5]*State Key Laboratory of Magnetic Resonance and Atomic and Molecular Physics, Wuhan Institute of Physics and Mathematics, Chinese Academy of Sciences, Wuhan 430071, China*

(Received 19 November 2010; published 30 March 2011)

We theoretically demonstrate the generation of wavelength-tunable, narrow-bandwidth extreme-ultraviolet (xuv) radiation by high-order harmonic generation (HHG) driven by an orthogonally polarized two-color laser field, which is composed of a 10-fs, 1500-nm laser pulse and a 40-fs, 2400-nm laser pulse. By performing classical analysis, we reveal that the rapid change of electron wave-packet dynamics at a subcycle time scale confines high-order harmonic emission to a small spectral region, leading to the generation of narrow-bandwidth xuv radiation. Furthermore, the central wavelength of the xuv radiation can be continuously tuned over a wide range by changing either the peak intensity of the driver laser or the amplitude ratio between the two laser fields at different wavelengths. It is also verified that the use of driver pulses at longer wavelengths leads to a better spectral confinement of the xuv radiation.

DOI: 10.1103/PhysRevA.83.033835 PACS number(s): 42.65.Ky, 42.65.Re

I. INTRODUCTION

High-order harmonic generation (HHG) [1–3], as a promising method to create table-top coherent extreme-ultraviolet (xuv) and x-ray sources as well as to synthesize attosecond pulses, has attracted great attention in the last two decades. In particular, in recent years, the rapid development of optical parametric amplifier (OPA) technology motivates the investigations of HHG [4–12] and strong field physics [13] with the mid-infrared laser pulses. In combination with the traditional ultrafast lasers operated at ∼800-nm wavelength, the tunable ultrafast laser sources provided by OPA also facilitate HHG in wave-form-controlled two-color laser fields. HHG driven by two-color fields has been intensively investigated in order to obtain higher xuv flux, higher cutoff energy, broader xuv supercontinuum, and so forth [10–12,14–21] Typically, high-order harmonic emission consists of a few rapidly decreasing harmonics followed by a plateau with a sharp cutoff at $I_p + 3.17U_p$ (where I_p is the ionization potential and U_p the ponderomotive energy) [22], so that the HHG spectrum always covers a considerably broad spectral range. On the other hand, wavelength-tunable xuv radiation with a narrow spectral bandwidth is of potential importance in many fields such as three-dimensional (3D) biological imaging, nanolithography, xuv interferometry, and so on. In order to create this kind of coherent light source via HHG, a series of methods have been explored. The most straightforward method is to use a filter or grating to spectrally select the desirable spectral components of the input beam [23,24]. However, these optical elements usually will induce a significant absorption or diffraction loss in the xuv regime. Another approach to obtain narrow-bandwidth xuv radiation from HHG is to precisely control the phase matching by carefully tailoring the shape of driver pulses in a feedback system [25] or by performing a quasi-phase-matching technique [26,27]. However, these methods based on phase matching are usually complex and difficult to implement. Fortunately, HHG driven by a parallel-polarized two-color field shows great potential to select and control a high-order harmonic spectrum [28,29]. Besides, Sansone *et al.* have recently demonstrated the spectral tuning of attosecond pulses by a polarization gating technique [30]. However, for these methods, the tunable spectral range is narrow.

In this paper, we theoretically demonstrate the generation of wavelength-tunable, narrow-bandwidth xuv radiation via HHG driven by an orthogonal-polarized two-color laser field and reveal the underlying physics by performing classical analysis. Our technique relies on control of the electron wave-packet dynamics at a subcycle time scale. Namely, in our technique, by two-color wave-form control only the electron ionized at a specific phase in the light field can be driven back to the parent ion while the electron ionized at the other phases cannot. From the semiclassical picture of HHG [22], in such a case, the electron that can recombine with the parent ion will only possess one kinetic energy, which in turn gives rise to the narrow-bandwidth xuv radiation with a clean background, because generation of the harmonics at all the other frequencies by the electron ionized at the other phases is prohibited.

II. MODEL AND NUMERICAL METHOD

In our simulation, the driver field consists of an intense 1500-nm, 10-fs laser field polarized in the x direction and a

*ycheng-45277@hotmail.com
†chen_jing@iapcm.ac.cn
‡zzxu@mail.shcnc.ac.cn

relatively weak 2400-nm, 40-fs laser field polarized in the y direction. The synthesized field can be expressed as

$$\vec{E}_s = E \exp\left[-2\ln(2)t^2/\tau_1^2\right]\cos(\omega_1 t)\cdot\hat{x} + AE \times \exp\left[-2\ln(2)(t-T_d)^2/\tau_2^2\right]\cos[\omega_2(t-T_d)]\cdot\hat{y}. \quad (1)$$

Here, ω_i and τ_i ($i = 1,2$) denote angular frequency and pulse duration of 1500-nm ($i = 1$) and 2400-nm ($i = 2$) fields, respectively. The parameters A and T_d are the amplitude ratio and time delay between the two fields, respectively. It is well known that the high-order harmonic signal is determined by the quantum-mechanical expectation value of dipole acceleration. The intensity of the nth harmonic from a single atom is proportional to $\omega_n^4 \cdot |\vec{d}_n|^2$ [31], where ω_n is the frequency of the generated xuv photon, and $\vec{d}_n$ the corresponding Fourier component of the field-induced dipole moment, which is calculated using the Lewenstein model [32]. The atom used in the numerical simulation is neon.

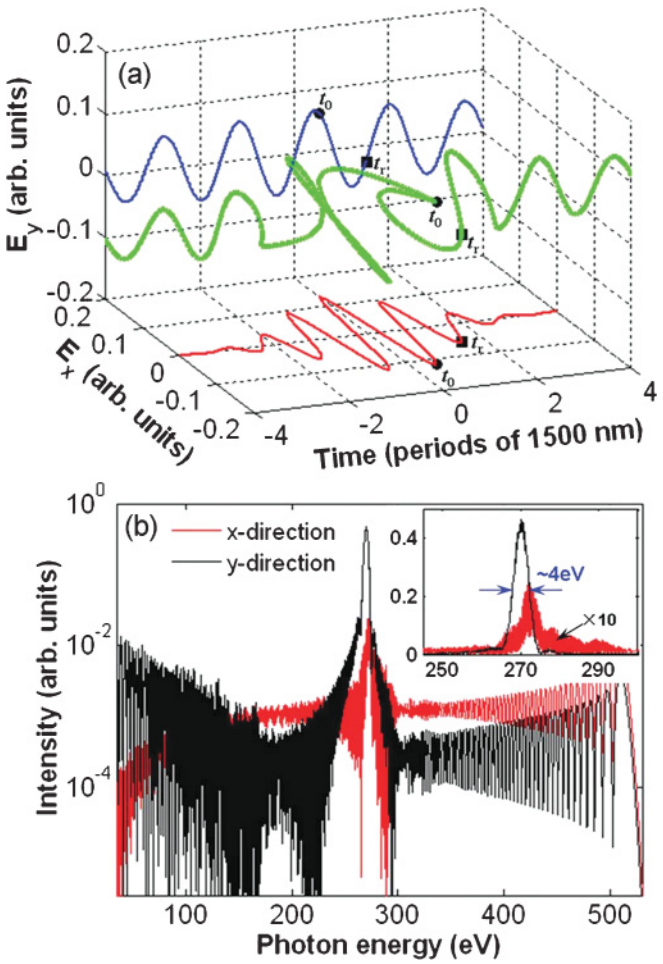

FIG. 1. (Color online) (a) 3D plot of the driver laser field synthesized by a 1500-nm, 10-fs laser field polarized in the x direction and a 2400-nm, 40-fs laser field polarized in the y direction. The amplitude ratio and time delay between the two laser fields are 0.5 and ~2.17 fs, respectively. (b) The x (red curve) and y components (black curve) of high-order harmonic spectra generated by the synthesized field in (a), showing that the x component is much weaker than the y component. Inset: High-order harmonic spectra in a linear scale.

III. THE GENERATION OF NARROW-BANDWIDTH xuv RADIATION AND CLASSICAL-TRAJECTORY ANALYSIS

In our simulation, the intensity of 1500-nm laser field is fixed at 6×10^{14} W/cm^2. The amplitude ratio and time delay between the 1500-nm and 2400-nm laser fields are set to be 0.5 and ~2.17 fs, respectively. The evolution of the synthesized electric field in 3D space is shown by the green curve in Fig. 1(a). Its x and y components are indicated by red and blue curves, respectively. Clearly, in the superimposing region of the two laser fields, the polarization state of the laser field exhibits a rapid and complex variation within an optical cycle. The high-order harmonic spectra in the x and y directions obtained with the driver field are shown by red and black lines in Fig. 1(b), respectively. Surprisingly, both the x and y components of harmonic spectra show a peak around 270 eV. In this way, xuv radiation with a limit bandwidth is well selected from the broad plateau region of the high-order harmonic spectrum. To give a clear demonstration, the harmonic spectra polarized in both the x and y directions are shown in linear scale [see inset of Fig. 1(b)]. As one can see, in the y polarization, the spectrum of the selected xuv radiation shows a smooth profile and a bandwidth of ~4 eV [full width at half maximum (FWHM)], which allows us to synthesize isolated pulses with subcycle duration. However, the xuv radiation in the x direction, which has a broad spectrum with deep modulations, is more than one order of magnitude weaker than that in the y direction.

In order to gain insight into the physics underlying the narrow-bandwidth emission of high-order harmonics, we perform classical analysis based on the three-step model of HHG [22]. Figure 2(a) shows the minimum returning distance of an electron (blue solid curve) and its returning kinetic energy (red dashed curve) as a function of birth time (i.e., the time at which the electron is tunnel ionized). It can be seen that only the electron born at t_0 (indicated by a red dot) can accurately return to its parent ion (i.e., its minimum returning distance approaches zero). When the electron is ionized slightly before or after t_0, the minimum returning distance of the electron rapidly increases. Quantum mechanically, due to the spreading of the electron wave packet, the electron with a displacement less than the radius of the electron wave packet will still have a decent probability to recombine with its parent ion and can emit high-harmonic photons. However, if the displacement is too large to be compensated for by the spreading of the electron wave packet, the electron will miss its parent ion. In this case, HHG efficiency will be largely reduced. Therefore, the dominant contribution to the high-order harmonic emission comes from the electrons born within a small time window centered at t_0, as indicated by the rectangle (shaft-gradient color filled) in Fig. 2(a). Furthermore, these electrons contributing to HHG have nearly the same returning kinetic energy, ~250 eV. Consequently, high-order harmonics can only be efficiently generated in a small spectral range around 270 eV. For a better understanding of the electron motion in the specific laser field, in Figs. 2(b)–2(d) we depict two-dimensional (2D) classical trajectories for the electrons born at $t_0-0.05$fs, t_0, and $t_0+0.05$ fs, respectively. The electron born at t_0 comes back to its initial position (the initial

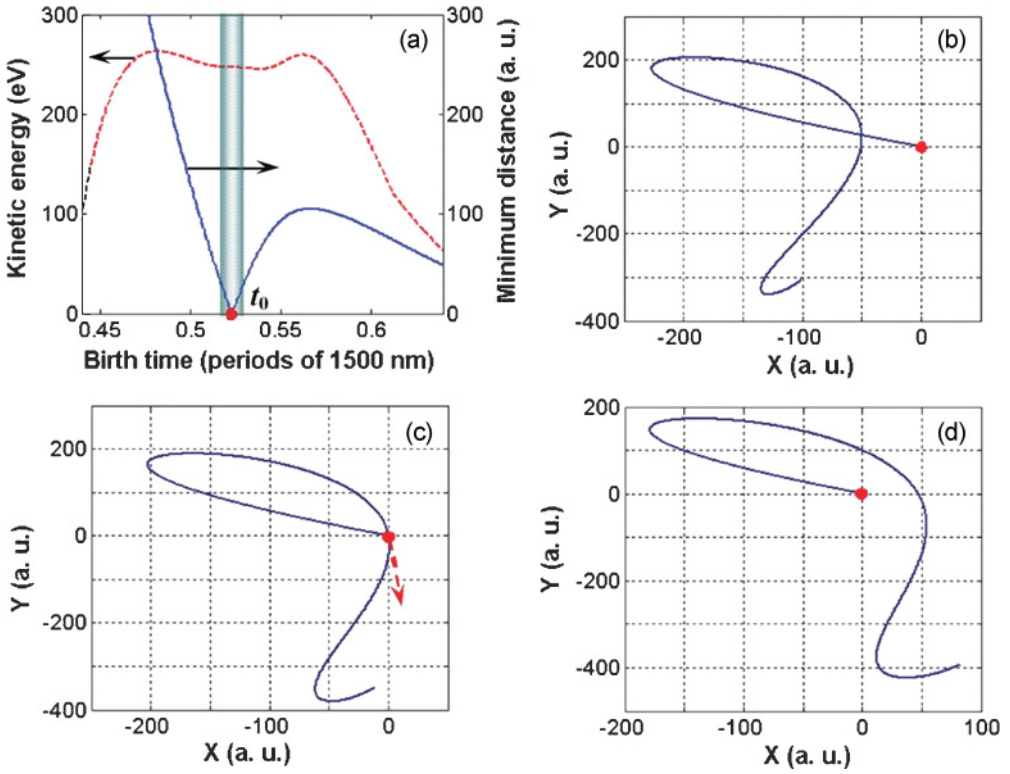

FIG. 2. (Color online) (a) Return kinetic energy (red dashed curve) and minimum returning distance of electron (blue solid curve) as a function of birth time; 2D classical trajectories for electrons born at the times (b) $t_0 - 0.05$ fs, (c) t_0, and (d) $t_0 + 0.05$ fs. Initial position of the electron is indicated by a red solid dot in all figures, and the motion direction of the recolliding electron is indicted by red arrows in (c).

position is indicated by the red solid dots) at t_r along a curved trajectory [see Fig. 2(c)] and then a high-energy photon with an energy equal to the kinetic energy plus the ionization potential can be generated when the electron is captured by the parent ion. We also notice that the recolliding electron moves in a direction nearly parallel to the y axis, as indicated by the red arrow in Fig. 2(c). Accordingly, the birth time (t_0) and the return time (t_r) of the electron are indicated by the black dots and black squares in Fig. 1(a), respectively. As shown in Fig. 1(a), because the recolliding electron is born near the peak of the electric field, and then recombines with its parent ion when the strength of electric field is near zero, the polarization direction of high-order harmonic emission can be considered to be the same as the direction of the electron motion (i.e., the high-order harmonic emission from the trajectory is polarized almost along the y axis) [33]. When the electron is ionized 0.05 fs before or after t_0, the minimum distances between the return electron and its parent ion reach up to ∼50 atomic units (a.u.), as illustrated in Figs. 2(b) and 2(d). Therefore, in these two cases, harmonic emission will significantly decrease or even terminate because of a great drop in recombination probability. The classical analysis given above clearly reveals that by controlling the electron wave-packet dynamics in the two-color driver field, HHG can be confined within a narrow spectral region.

IV. TUNABILITY OF THE CENTRAL WAVELENGTH

In this section, we first investigate how the total high-order harmonic spectra (defined as the summation of spectral intensities in the x and y directions) changes with an increasing laser intensity while both amplitude ratio and time delay between the two fields remain unchanged. When the laser intensity of 1500-nm pulses increases from 3×10^{14} to 9×10^{14} W/cm^2, the selected xuv radiation gradually shifts to higher photon energy, covering a wide tuning range from ∼150 to ∼400 eV, as illustrated in Fig. 3(a). According to the three-step model of HHG [22], with the increase of laser intensity, the recolliding electron will obtain higher kinetic energy from the laser field, leading to xuv radiation at higher photon energy. Interestingly, the selected harmonics generated at different driver laser intensities have nearly the same peak intensity and the same bandwidth, which allows us to create a wavelength-tunable xuv source only by removing all the low-order harmonics using a thin metal foil (e.g., a piece of silver foil).

Next, we fix the intensity of 1500-nm pulses at 6×10^{14} W/cm^2 and adjust the intensity of the 2400-nm laser pulses by tuning the amplitude ratio of the two laser fields (A). With the increase of the amplitude ratio, the narrow-bandwidth xuv radiation moves towards higher photon energy, as shown in Fig. 3(b). At $A = 0.2$, a sharp peak appears around ∼63 eV and there is still weak background emission in the spectral range from 70 to 230 eV. At $A = 0.5$, the selected spectral range is the narrowest and with the highest contrast. When A increases to 0.6 or even higher, the harmonic spectrum shows a significant modulation, which should be the result of the interference between high-order harmonics from different quantum trajectories [34]. Thus, in order to obtain a tunable and spectrally smooth xuv source, the amplitude ratio between the two laser fields can only be chosen within a certain range.

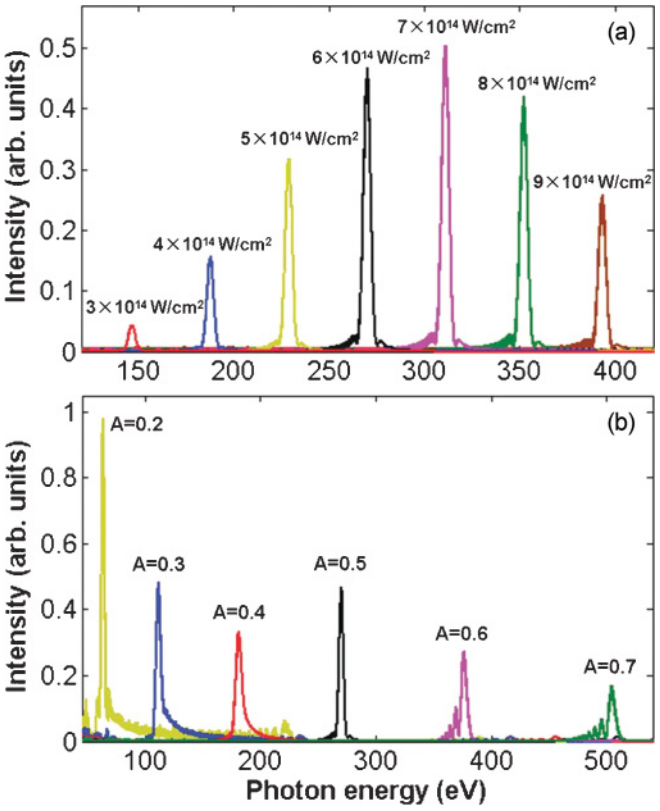

FIG. 3. (Color online) High-order harmonic spectra obtained (a) at different intensities of 1500-nm pulses from 3×10^{14} to 9×10^{14} W/cm^2 and (b) at different amplitude ratios ($A = 0.2$–0.7) between 1500- and 2400-nm pulses. The time delay is optimized to be ~2.17 fs.

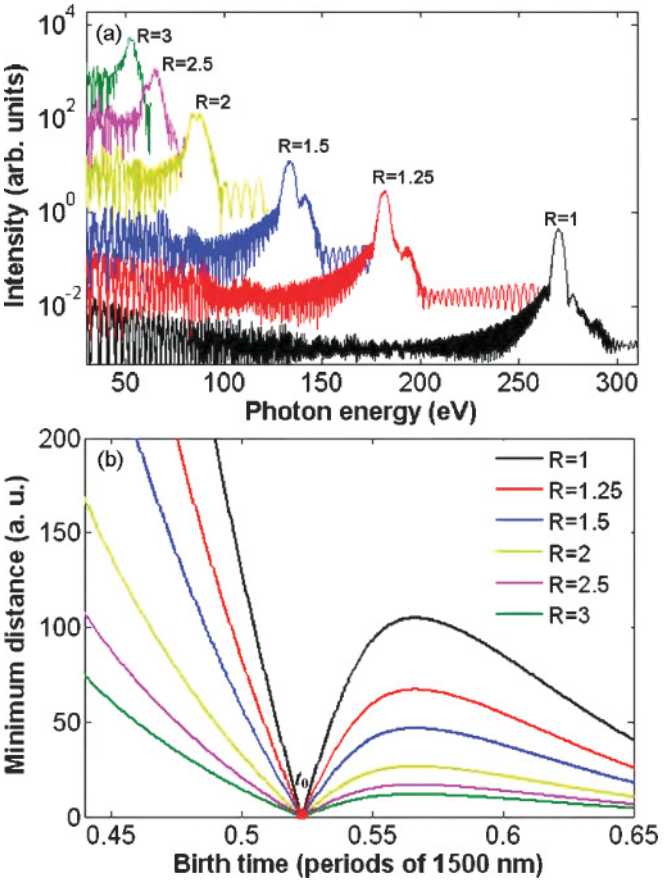

FIG. 4. (Color) (a) High-order harmonic spectra and (b) the minimum returning distance of the electron from its parent ion at different driver wavelengths ($R = 1$–3) when the time delay between the two fields is kept at ~0.27 optical period of the $2400/R$-nm laser field.

V. ROLE OF DRIVER WAVELENGTH

In order to further explore the physics behind the spectral selection, we study the influence of driver wavelength on the selective emission of high-order harmonics. To this end, the wavelengths of the two laser fields are adjusted simultaneously by a parameter R. Namely, we set one laser field as $1500/R$ nm, while the other $2400/R$ nm. As a consequence, the time delay between the two fields is kept at ~0.27 optical period of the $2400/R$-nm laser field, and the pulse durations of the short- and long-wavelength laser fields are set to be 2 and 8 optical periods of the $1500/R$-nm laser field, respectively. High-order harmonic spectra obtained at different driver wavelengths are illustrated in Fig. 4(a). Clearly, the longer the driver wavelength, the narrower the bandwidth of the selected xuv. For gaining a deeper insight, we again perform the classic-trajectory analyses by studying the minimum returning distance of the electron at different driver wavelengths. As shown in Fig. 4(b), for any driver wavelength, the electron born at t_0 will return to its original position. In the case of the longest wavelength used (i.e., $R = 1$), a small variation in birth time causes a most significant increase of minimum returning distance. On the contrary, in the case of a short-wavelength driver field (i.e., $R = 3$), the minimum returning distance of the electron remains small in a broad range of birth time. Particularly, for the electron born after t_0, the minimum returning distance is below 12 a.u., and thus it will still have the probability to generate high-order harmonics. At a given birth time, minimum returning distance of the electron is approximately proportional to the square of the driver wavelength (i.e., reversely proportional to R^2). On the other hand, it is also known that the excursion time of the electron in the continuum and thus wave-packet spreading is proportional to the driver wavelength, assuming a constant spreading rate of the electron wave packet. As we have shown in our previous investigation [7], the interplay between the electron displacement and the spreading of the electron wave packet at longer driver wavelengths leads to a sharper dependence of the HHG efficiency on the ellipticity of the driver field. This is exactly the underlying physics of why the narrower HHG spectrum can only be obtained at longer driver wavelengths. Moreover, with the increase of the driver wavelength, the tunable xuv radiation will move towards higher photon energy while its conversion efficiency drops dramatically. This is in good agreement with the wavelength scaling law of HHG efficiency, as has been reported by several research groups [35].

Because the key point of this technique is to create a driver field with a specific wave form by which only the electron born at a unique time has the capability to be driven back to the nucleus, the bandwidth of the tunable xuv sources should

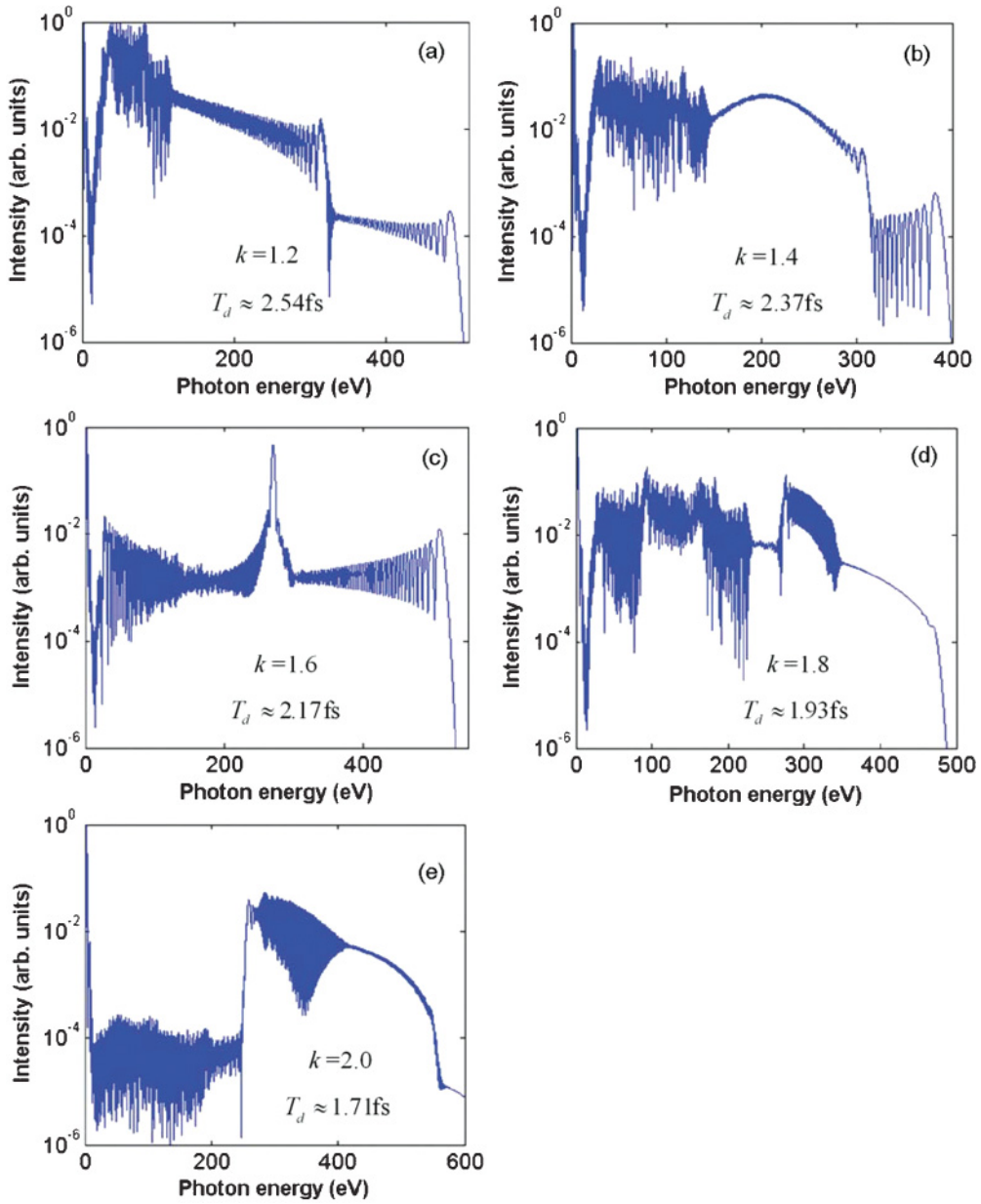

FIG. 5. (Color online) High-order harmonic spectra at different wavelength ratios: (a) $k = 1.2$, (b) $k = 1.4$, (c) $k = 1.6$, (d) $k = 1.8$, and (e) $k = 2.0$. For each ratio, the time delay T_d is optimized to achieve the narrowest bandwidth for the spectrum, as indicated in each figure.

naturally be sensitive to the ratio between the wavelengths of two laser fields, which determines the synthesized wave form. To verify this, we further investigate the influence of the wavelength ratio on the high-order harmonic spectra. In the calculation, we assume that one wavelength is 1500 nm, and the other $1500 \times k$ nm, where k is the ratio between the wavelengths of two laser fields. The peak intensities and amplitude ratio of the two driver fields are the same as those used in Fig. 1(b). The pulse durations of the two fields at 1500 nm and $1500 \times k$ nm wavelengths are 10 and 40 fs, respectively. For each wavelength ratio k, the time delay T_d (indicated in each part of Fig. 5) is optimized to achieve the narrowest bandwidth for the tunable xuv radiation. As shown in Fig. 5, the wavelength ratio is indeed critical, and the narrow-bandwidth high-order harmonic spectrum can only be obtained with an optimized wavelength ratio of $k = 1.6$.

Finally, we examine the feasibility of experimental demonstration of the generation of tunable, narrow-bandwidth xuv radiation using the above technique. For this purpose, we investigate sensitivity of the high-order harmonic spectra to the fluctuation of the pulse duration of the 1500-nm field, as well as to the jitter of the time delay between the 1500- and 2400-nm fields. By numerical simulation, we find that fluctuation of the pulse duration within ± 1 fs (i.e., 9 to $\sim$11 fs) can hardly influence the high-order harmonic spectrum (data not shown). Although it is challenging to stabilize the pulse duration within such a narrow window, it should still be technically achievable. In addition, the time delay of the two laser fields is also critical for obtaining the narrow-bandwidth

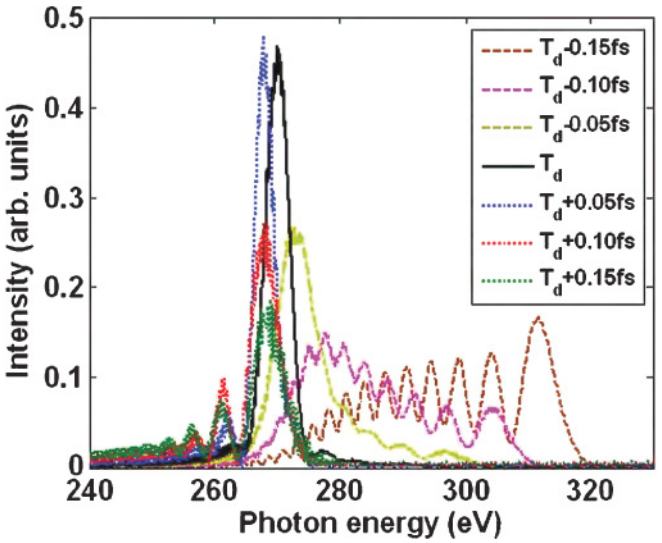

FIG. 6. (Color) High-order harmonic spectra obtained by fine tuning the time delay between the 1500- and 2400-nm laser fields at a step of 50 as. T_d is an optimized time delay (i.e., ∼2.17 fs). The amplitude ratio between the two laser fields is 0.5. Laser intensity of 1500-nm pulses is 6×10^{14} W/cm^2.

HHG. In Fig. 6, we show high-order harmonic spectra as a function of the time delay with a step of 50 as. Here, T_d is an optimized time delay (i.e., ∼2.17 fs). From the results, it is clear that the narrow-bandwidth xuv radiation can be observed for a time delay ranging from −50 as (yellow dashed curve) to +100 as (red dotted curve); however, the peak intensity of HHG will decrease with increasing time jitter. If the time jitter could be well controlled in a tighter range (e.g., ±25 as), the spectrum of tunable xuv radiation will remain almost unchanged. Thus, we expect that with the technique development, experimental demonstration of this phenomenon should be possible. And depending on the requirements of specific applications, this technique may find use in the future. Last but not least, with the mechanism shown in this work, one might be able to further optimize the parameter settings so that the experimental conditions or parameters can be less stringent.

VI. CONCLUSIONS

We propose a method to generate narrow-bandwidth, coherent xuv sources. By optimizing the time delay between the two orthogonal-polarized laser fields, high-order harmonics only can be efficiently generated in a narrow spectral range. The central wavelength of the selected xuv radiation can be easily controlled by adjusting laser parameters of the driver field. Classical analysis reveals that the rapidly varying electron motion in the two-color fields is the cause of the selective emission of high-order harmonics. Finally, it is particularly true that in many cases, phase matching can lead to the change of both the phase and spectral profile of the high-order harmonic due to the fact that the phase-velocity difference between the harmonic and the driver laser varies with the order of harmonic; however, in our scheme, the narrow bandwidth of the xuv emission makes it less sensitive to the propagation in terms of its spectral profile and its phase (e.g., chirp). In principle, our technique also could take advantage of the phase matching if the phase-matching condition is optimized for the wavelength of the narrow-bandwidth xuv emission. Such a narrow-bandwidth xuv source will have important applications in many fields of science and technology, such as nanolithography, xuv interferometry, biological imaging, and so on.

ACKNOWLEDGMENT

This work was supported by the National Natural Science Foundation of China (Grants No. 60921004, No. 11074026, No. 10974213, No. 11004209, and No. 60825406).

[1] F. Krausz and M. Ivanov, Rev. Mod. Phys. **81**, 163 (2009).
[2] G. Sansone *et al.*, Science **314**, 443 (2006).
[3] M. Schultze, E. Goulielmakis, M. Uiberacker, M. Hofstetter, J. Kim, D. Kim, F. Krausz, and U. Kleineberg, New J. Phys. **9**, 243 (2007).
[4] P. Colosimo *et al.*, Nat. Phys. **4**, 386 (2008).
[5] H. Xiong *et al.*, Opt. Lett. **34**, 1747 (2009).
[6] Y. Fu *et al.*, Phys. Rev. A **79**, 013802 (2009).
[7] H. Xu, H. Xiong, B. Zeng, W. Chu, Y. Fu, J. Yao, J. Chen, X. Liu, Y. Cheng, and Z. Xu, Opt. Lett. **35**, 472 (2010).
[8] E. J. Takahashi, T. Kanai, K. L. Ishikawa, Y. Nabekawa, and K. Midorikawa, Phys. Rev. Lett. **101**, 253901 (2008).
[9] H. Xu, H. Xiong, Z. Zeng, Y. Fu, J. Yao, R. Li, Y. Cheng, and Z. Xu, Phys. Rev. A **78**, 033841 (2008).
[10] Y. Yu, X. Song, Y. Fu, R. Li, Y. Cheng, and Z. Xu, Opt. Express **16**, 686 (2008).
[11] J. Yao *et al.*, Phys. Rev. A **82**, 023826 (2010).
[12] B. Zeng, Y. Yu, W. Chu, J. Yao, Y. Fu, H. Xiong, H. Xu, Y. Cheng, and Z. Xu, J. Phys. B **42**, 145604 (2009).
[13] W. Quan *et al.*, Phys. Rev. Lett. **103**, 093001 (2009).
[14] T. Siegel *et al.*, Opt. Express **18**, 6853 (2010).
[15] F. Calegari *et al.*, Opt. Lett. **34**, 3125 (2009).
[16] T. Pfeifer, L. Gallmann, M. J. Abel, P. M. Nagel, D. M. Neumark, and S. R. Leone, Phys. Rev. Lett. **97**, 163901 (2006).
[17] H. Merdji, T. Auguste, W. Boutu, J.-P. Caumes, B. Carré, T. Pfeifer, A. Jullien, D. M. Neumark, and S. R. Leone, Opt. Lett. **32**, 3134 (2007).
[18] P. Lan, P. Lu, Q. Li, F. Li, W. Hong, and Q. Zhang, Phys. Rev. A **79**, 043413 (2009).
[19] H.-C. Bandulet, D. Comtois, E. Bisson, A. Fleischer, H. Pépin, J.-C. Kieffer, P. B. Corkum, and D. M. Villeneuve, Phys. Rev. A **81**, 013803 (2010).
[20] L. E. Chipperfield, J. S. Robinson, J. W. G. Tisch, and J. P. Marangos, Phys. Rev. Lett. **102**, 063003 (2009).
[21] Z. Zeng, Y. Cheng, X. Song, R. Li, and Z. Xu, Phys. Rev. Lett. **98**, 203901 (2007).
[22] P. B. Corkum, Phys. Rev. Lett. **71**, 1994 (1993).

[23] L. B. Da Silva *et al.*, Phys. Rev. Lett. **74**, 3991 (1995).
[24] J. B. M. Warntjes, A. Gürtler, A. Osterwalder, F. Rosca-Pruna, M. J. J. Vrakking, and L. D. Noordam, Opt. Lett. **26**, 1463 (2001).
[25] R. Bartels, S. Backus, E. Zeek, L. Misoguti, G. Vdovin, I. P. Christov, M. M. Murnane, and H. C. Kapteyn, Nature (London) **406**, 164 (2000).
[26] X. Zhang, A. L. Lytle, T. Popmintchev, X. Zhou, H. C. Kapteyn, M. M. Murnane, and O. Cohen, Nat. Phys. **3**, 270 (2007).
[27] A. L. Lytle, X. Zhang, P. Arpin, O. Cohen, M. M. Murnane, and H. C. Kapteyn, Opt. Lett. **33**, 174 (2008).
[28] Z. Zeng, Y. Cheng, Y. Fu, X. Song, R. Li, and Z. Xu, Phys. Rev. A **77**, 023416 (2008).
[29] E. Mansten, J. M. Dahlström, P. Johnsson, M. Swoboda, A. L'Huillier, and J. Mauritsson, New J. Phys. **10**, 083041 (2008).
[30] G. Sansone, E. Benedetti, C. Vozzi, S. Stagira, and M. Nisoli, New J. Phys. **10**, 025006 (2008).
[31] M. Y. Ivanov, T. Brabec, and N. Burnett, Phys. Rev. A **54**, 742 (1996).
[32] M. Lewenstein, Ph. Balcou, M. Y. Ivanov, A. L'Huillier, and P. B. Corkum, Phys. Rev. A **49**, 2117 (1994).
[33] Ph. Antoine, B. Carré, Anne L'Huillier, and M. Lewenstein, Phys. Rev. A **55**, 1314 (1997).
[34] A. Zaïr *et al.*, Phys. Rev. Lett. **100**, 143902 (2008).
[35] J. Tate, T. Auguste, H. G. Muller, P. Salières, P. Agostini, and L. F. Di Mauro, Phys. Rev. Lett. **98**, 013901 (2007).